



LAWRENCE
LIVERMORE
NATIONAL
LABORATORY

Reflected Blast Wave Environments from C-4 Charges

W. M. Howard, A. L. Kuhl, K. S. Vandersall, F.
Garcia, D. W. Greenwood

March 8, 2010

14th International Detonation Symposium
Coeur d'Alene, ID, United States
April 11, 2010 through April 16, 2010

Disclaimer

This document was prepared as an account of work sponsored by an agency of the United States government. Neither the United States government nor Lawrence Livermore National Security, LLC, nor any of their employees makes any warranty, expressed or implied, or assumes any legal liability or responsibility for the accuracy, completeness, or usefulness of any information, apparatus, product, or process disclosed, or represents that its use would not infringe privately owned rights. Reference herein to any specific commercial product, process, or service by trade name, trademark, manufacturer, or otherwise does not necessarily constitute or imply its endorsement, recommendation, or favoring by the United States government or Lawrence Livermore National Security, LLC. The views and opinions of authors expressed herein do not necessarily state or reflect those of the United States government or Lawrence Livermore National Security, LLC, and shall not be used for advertising or product endorsement purposes.

Reflected Blast Wave Environments from C-4 Charges

William M. Howard* and Allen L. Kuhl^{f,*}
Kevin S. Vandersall*, Frank Garcia* and Daniel W. Greenwood*

* Energetic Materials Center

^f AX Division, WCI

Lawrence Livermore National Laboratory
7000 East Ave., Livermore, CA 94551 USA

Abstract. We use an Arbitrary-Lagrange-Eulerian (ALE3D) hydrodynamics code to calculate the reflection of a spherical, high explosive (HE)-driven blast wave from an ideal plane surface. For the high explosive, we assume a C4 charge. We use a finely resolved 2-D mesh (50 zones/cm) to capture the blast wave propagation and its interaction with the air as well as its subsequent reflection from the ideal planar surface. The propagation is followed for a distance to 43.0 cm. We use both an Eulerian scheme and a 2nd order advection scheme that maps from a Lagrangian to an Eulerian mesh. We use an equilibrium (program) burn Cheetah model for the detonation, as well as a JWL equation of state (EOS). We first employed a Livermore Equation of State (LEOS) for the air. This EOS for the air is valid to kilo-volt temperatures and includes effects of ionization. However, we found that using an equilibrium Cheetah model for air gave a more accurate representation of the pressures in the temperature range of interest ($T \sim 5000\text{K}$ to 8000K). We perform experiments in a 506 liter barometric calorimeter with fourteen pressure gauges spaced at two inch intervals along the top of the calorimeter. Our model results agree quite well with the responses of the pressure gauges for a C4 explosive charge.

Introduction

One could say that the scientific framework of explosions began in 1950 with Sir G. I. Taylor's seminal publication¹ on similarity solutions for planar and spherical Chapman-Jouguet detonation waves in condensed explosives. This methodology was codified by Zel'dovich and Kompaneets in their book on the *Theory of Detonation*², first published in 1955. It was Hal Brode who in 1955-1959 first computed the one-dimensional blast wave generated by the detonation of a spherical TNT charge in air³ using a 1D Lagrangian finite difference code. It was Anisimov and Zel'dovich⁴

who first pointed out the growth of Rayleigh-Taylor instabilities on the detonation products-air interface in 1977. The transition of these instabilities into a spherical turbulent mixing layer was studied by Kuhl⁵ in 1996 via direct numerical simulations with a three-dimensional (3D) gasdynamics code based a high-order Godunov scheme^{6,7} with adaptive mesh refinement (AMR)⁸ to capture the mixing structures. This same technique was used to study the reflection of a blast wave from a spherical PBX-9404 charge⁹ in the high-pressure (~ 1 k-bar) regime.

By now, the subject of air blast effects is quite mature—as evidenced by the books by Kinney¹⁰

REFLECTED BLAST WAVES FROM C-4 CHARGES

and Baker¹¹, as well as the applications handbooks by Swisdak¹² and Petes¹³ to name just a few.

More recently, Kuhl and Reichenbach have developed a barometric calorimeter¹⁴ technique to study combustion effects in confined explosions¹⁵ from 1.5 gram TNT charges and 1.5 gram aluminized-fuel charges. Evolution of combustion in those experiments has been successfully modeled^{16, 17} with a two-phase version of the previously mentioned AMR code.

This barometric calorimeter technique has been scaled up from 6.6 liters to a 506-liter chamber, which can accommodate 100-g charges. Here we report results of pressure measurements of the reflected blast wave from 50-g C-4 charges, and the numerical simulation of those experiments performed with our ALE3D hydrocode¹⁸.

Experiments

Experiments were performed in our barometric calorimeter. The chamber was a right circular cylinder (Fig. 1) with 5 cm thick steel walls and interior dimensions of $D = H = 86$ cm, and a volume of 506 liters. The lid was secured to the chamber body with twenty-four 5 cm diameter steel bolts; a rubber gasket was used to create a sealed pressure vessel. In this way the chamber was designed to accommodate steady state pressures of 12 bars (~100 g charges, including afterburning effects). During testing, the calorimeter was placed inside our 1-kg tank, and the chamber door was closed for safety considerations.

The principal diagnostic consisted of eight Kistler 603B piezo-electric pressure gauges located on the chamber lid at: at $r = 0$ and at $r = 5, 10, 15, 20, 25$ and 30 cm. Signals were recorded on a Yokogawa DL-750 digital storage system at 10 mega-samples per second and 12-bit resolution.



Figure 1. 506-liter barometric calorimeter installed in the 1-kg tank.

In this test series, 50-g C4 charges were used as the explosive source. The putty-like charge was filled in a plastic bag to serve as a container, and then formed into a spherical shape. It was securely strapped to a plastic supporting bracket (Fig. 2) containing an SE-1 detonator (similar to RP-1). The charge center was located in the center of the chamber (43 cm from the reflecting lid).



Figure 2. 50-g C4 charge and mounting bracket.

First, two calibration tests were fired with the RP-2 detonator to check the electronics system. Then two tests were conducted with 50-g C-4 charges detonated in an air atmosphere. Pressure histories will be presented in the **Results** section, and compared with the numerical simulations.

Numerical Simulations

We used the Arbitrary-Lagrange-Eulerian (ALE3D) hydrodynamics code¹⁸ to calculate the detonation of the C-4 charge, the expansion of the detonation products to form a blast wave in air,

and the subsequent reflections of that blast wave from the chamber lid and walls.

Initial Conditions

We assumed 2-D symmetry, so the computational domain ($0 < r < 43$ cm by $-2 < z < 43$ cm) was only one quarter of the chamber volume (Fig. 3); the cylinder axis of the chamber is shown in the horizontal position in this and all subsequent figures. A uniform finely resolved (50 cells/cm) fixed Eulerian mesh was used: 2,150 r-cells by 2,250 z-cells. The left, right and top computational boundaries ($z = -2$ cm, $z = 43$ cm and $r = 43$ cm, respectively) were treated as ideal reflecting planes; the $r = 0$ boundary was treated as an axis of symmetry. The center of C-4 charge was placed at $r = z = 0$, tangent to the left wall ($z = -2$ cm), which modeled the mounting bracket shown in Fig. 2. The charge was initiated at its left boundary ($r = 0, z = -2$ cm); a programmed burn model²¹, with a detonation velocity of 7.9 km/s was used to model the effects of the RP-2 initiator.

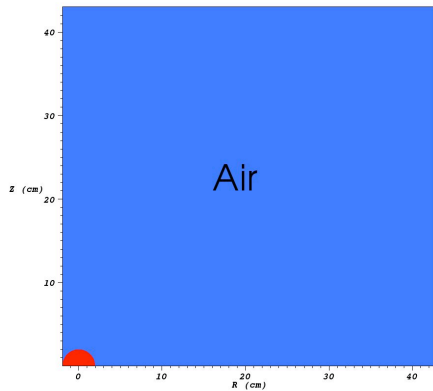


Figure 3. Initial conditions showing the computational domain and the C4 charge.

Equation of State (EOS)

As a baseline, we used the Cheetah code¹⁹ as subroutine to supply the thermodynamic properties of the C-4 detonation products gases, which are needed to define the equations of state (EOS) in

the ALE code simulations. The locus of thermodynamic states of the C-4 detonation products gases in the specific internal energy-temperature plane and in the pressure-specific volume plane are displayed in Figs. 4 and 5, respectively. These loci come from Cheetah code¹⁹ calculations, and are reported in a companion paper²⁰ in this Symposium. Air was also modeled with an equilibrium Cheetah model that takes into account molecular dissociation of nitrogen to N and NO, but not ionization.

Some simulations used the JWL equation of state for the detonation products and a perfect gas law for air (with $\gamma = 1.4$). By comparing pressure histories from the two calculations, one can determine quantitatively the influence of different EOS models.

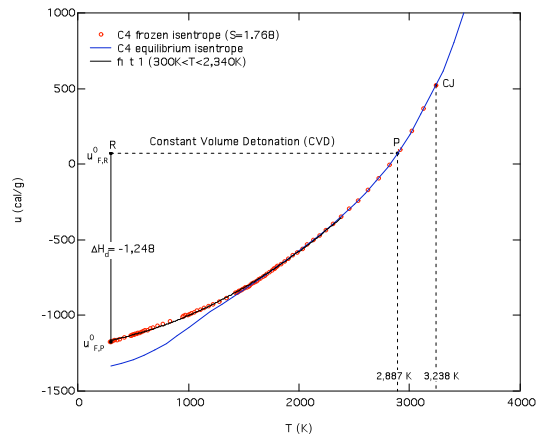


Figure 4. *Le Chatelier* diagram depicting the locus of states of the C-4 detonation products, starting at the *Chapman-Jouguet* point (*CJ*) point and expanding at constant entropy to one atmosphere²⁰.

REFLECTED BLAST WAVES FROM C-4 CHARGES

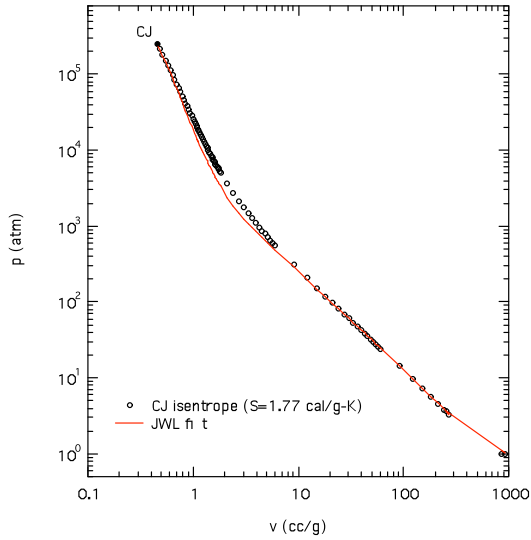


Figure 5. Pressure-volume diagram depicts the locus of states of the C-4 detonation products gases as they expand down the CJ isentrope²⁰.

Results

Flow Visualization

A cross-section of the material composition field at 275 μ s is shown in Fig. 6. The detonation products-air interface is unstable (as pointed out by Anisimov and Zel'dovich⁴) and has developed Richtmyer-Meshkov structures. Figure 7 depicts the corresponding temperature field at 275 μ s. The interface region has evolved into a spherical mixing layer shell⁵, bounded by the main shock and the inner (imploding) shock³. The blast wave has reflected from the surface, and a regular-reflection structure is evident in the region $0 < r < 18$ cm. The temperature field at 593 μ s is presented in Fig. 8. By this time, shock reflections from the walls have deposited baroclinic vorticity throughout the chamber, so virtually all the flow is turbulent.

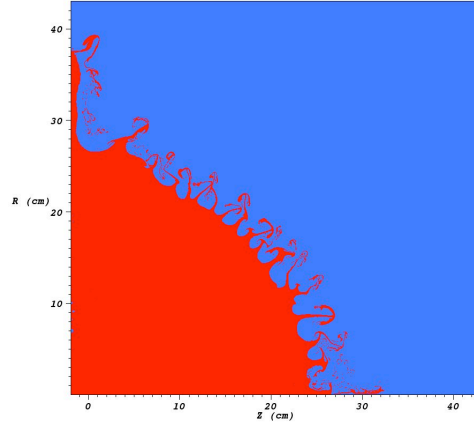


Figure 6. Material composition field at 275 μ s.

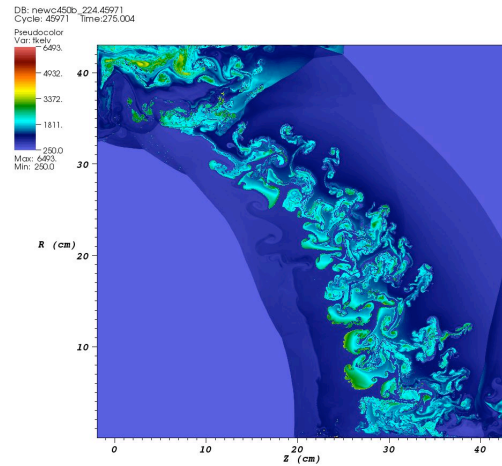


Figure 7. Temperature field at 275 μ s.

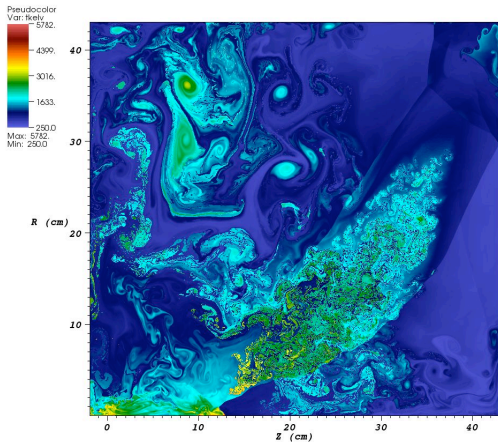


Figure 8. Temperature field at 593 μ s.

Free Air Curve

The incident shock over-pressure was sampled from the calculation as the blast wave expanded. The results are shown as the free-air curve of shock over-pressure versus scaled radius: R ($\text{cm}/\text{g}^{1/3}$) in Fig. 10.

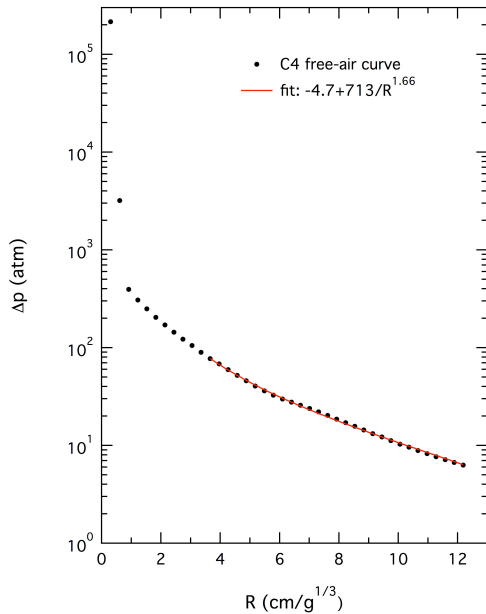


Figure 9. Free-air curve for C-4 (from 2-D ALE simulation along 45 deg. diagonal).

The curve was fit with the inverse power law function:

$$\Delta p(\text{atm}) = -4.7 + 713/R^{1.66} \tag{1}$$

This gives an incident shock over-pressure of 13 bars at ground zero ($z = 43$ cm, $r = 0$); upon reflection, ground zero will experience a peak pressure of 40 bars.

Waveforms

The pressure histories from the calculation were sampled at the seven gauge locations on the wall ($GR = 0, 2, 4, \dots, 30$ cm), and stored. These computed waveforms are compared with the measured pressure histories in Figs. 10-16. ALE results are shown as blue curves, while tests 3 and 4 are shown as black and red curves, respectively.

At ground zero ($GR = 0$), tests 3 and 4 give remarkably similar waveforms for the first, second and third blast waves. However, blast wave from the simulation is much too strong (e.g. by a factor of 2 in shock pressure), and quite noisy. This enhanced peak pressure is due to artificial (numerical) jetting along the $r = 0$ axis (see Fig. 6), while the noise comes from shock reflections off the turbulent mixing structures on the fireball interface (see Fig. 7), and is qualitatively realistic—although more pronounced than in the experiments.

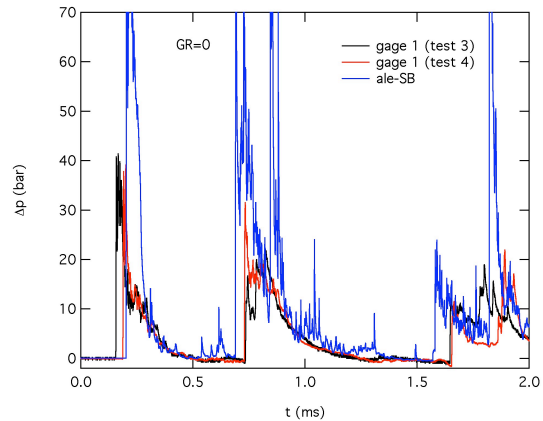


Figure 10. Computed pressure history (blue curve) vs. measured waveforms ($GR=0$).

REFLECTED BLAST WAVES FROM C-4 CHARGES

Stating at a ground range $GR = 5$ cm, the effects of jetting along the axis have subsided, and the computed waveform is similar to the measurements; the double-shock structure evident in the second and third blast waves in the experiments is captured qualitatively in the simulation. This qualitative similitude is also observed at the larger ground ranges, as shown in Figs. 12-16. However, some records (notably $GR = 10$ cm, test 3; $GR = 15$ cm, test 3 and 4; $GR = 25$ cm, test 3; $GR = 30$ cm, test 4) experienced unphysical under-shoots (un-realistic negative pressures) due to thermal effects on the piezoelectric sensors. In future tests, we plan to use more thermal shielding, and also use piezoresistive gauges (Kistler 4075A) to overcome this problem.

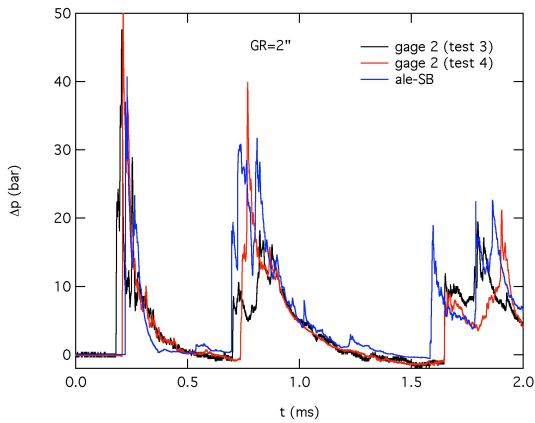


Figure 11. Computed pressure history (blue curve) vs. measured waveforms ($GR=5$ cm).

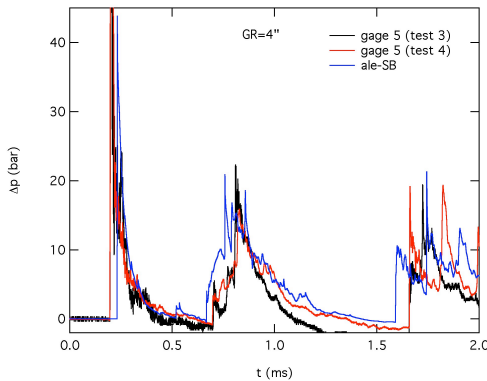


Figure 12. Computed pressure history (blue curve) vs. measured waveforms ($GR=10$ cm).

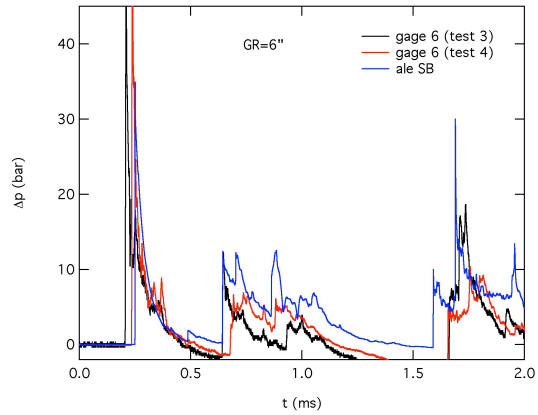


Figure 13. Computed pressure history (blue curve) vs. measured waveforms ($GR=15$ cm).

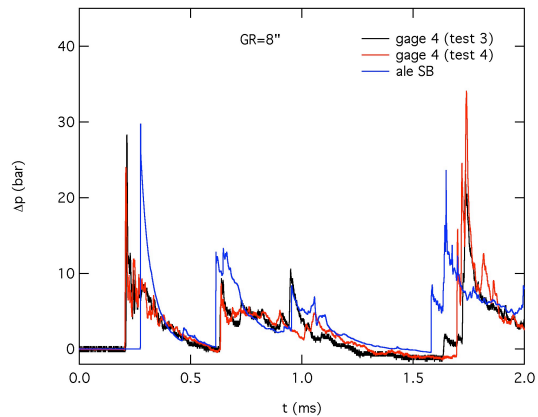


Figure 14. Computed pressure history (blue curve) vs. measured waveforms ($GR=20$ cm).

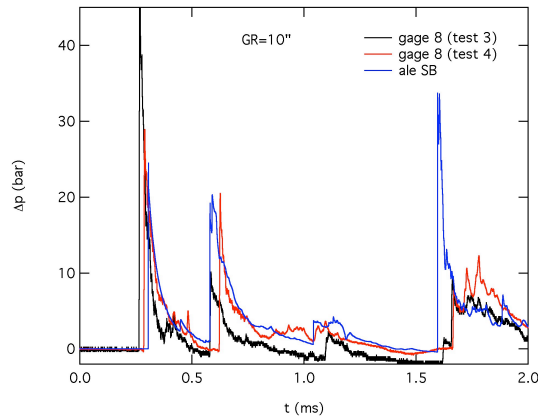


Figure 15. Computed pressure history (blue curve) vs. measured waveforms ($GR=25$ cm).

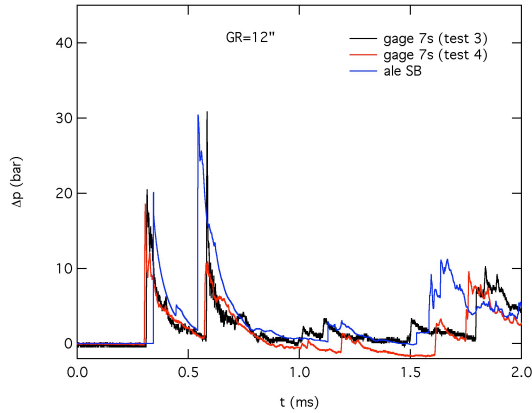


Figure 16. Computed pressure history (blue curve) vs. measured waveforms (GR=30cm).

Positive-Phase Impulse

The waveforms from Figs. 10-16 have been integrated to evaluate the positive phase impulse, I_+ , according to:

$$I_+(GR) = \int_0^{\tau_+} \Delta p(GR, t') dt' \quad (2)$$

where τ_+ denotes the positive phase of the primary (first) blast wave. Results are presented in Fig. 17. The calculated impulse at ground zero is 2.5 times larger than the experiment, as a consequence of the enhanced peak pressure (Fig. 10) caused by the numerical jetting on the axis (Fig. 6). At other ground ranges, impulses from the computed waveforms agree with the lower bound of the experimental impulses.

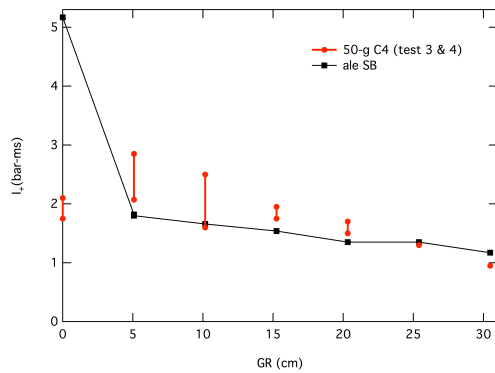


Figure 17. Positive phase impulse history versus ground range: calculation vs. experiments.

Discussion

We have also performed ALE3D code simulations of 3.3-kg spherical PBX-9404 charge at 52 cm from the reflecting surface. This case is much closer to the surface ($HOB = 3.4 \text{ cm/g}^{1/3}$) than the C-4 case ($HOB = 11.7 \text{ cm/g}^{1/3}$) reported here. The temperature field of the reflection process is shown in Fig. 18 at 130 μs . Peak temperatures in the turbulent mixing layer reach 6,000 K; peak pressures of 1-kbar were measured near ground zero⁹. Clearly one needs a complete EOS (a function of two thermodynamic variables) to properly characterize the thermodynamic properties of the gases under such extremes in pressure and temperature. Cheetah, employed as a EOS subroutine, does precisely this.

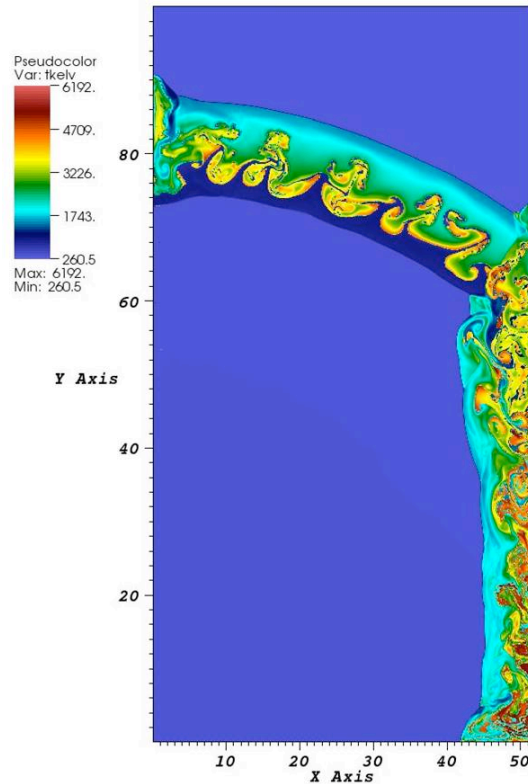


Figure 18. Reflection of a 3.6-kg spherical PBX-9404 charge at 52 cm ($HOB = 3.4 \text{ cm/g}^{1/3}$).

REFLECTED BLAST WAVES FROM C-4 CHARGES

Conclusions

The reflected blast wave environment was measured in the 506-liter bomb calorimeter for 50-g spherical C-4 charges suspended 43 cm from a reflecting surface ($HOB = 11.7 \text{ cm/g}^{1/3}$). Peak reflected pressures ranged from 40 bars at ground zero to 20 bars at $GR = 30 \text{ cm}$. The corresponding positive phase impulses varied from 3 bar-ms down to values of $\sim 1 \text{ bar-ms}$ over the same ground ranges. There was considerable variation ($\pm 50\%$) in the positive phase impulse at some ground ranges; this was certainly not the case in experiments with 1-g PETN spheres ($\pm 1-3\%$)¹⁴, so perhaps C-4 should not be used as a benchmark standard.

The reflected blast wave environment of the experiments was simulated with the ALE3D code. The thermodynamic states were specified by the Cheetah code, which was used as an EOS subroutine. Neglecting ground zero (which suffered from numerical jetting effects), the computed waveforms were similar to the measured waveforms; the computed positive phase impulse agreed with the lower bound of the measured impulse at various ground ranges.

As the charge is detonated closer and closer to the reflecting surface, real gas effects become more and more important. For example, at $HOB = 3.4 \text{ cm/g}^{1/3}$, peak pressures and temperatures can reach 1 k-bar and 6,000 – 9,000 K. The JWL function and γ -law gas models are inadequate for these circumstances. One needs a complete thermodynamic description of the gas properties, which are functions of two thermodynamic variables²⁰. The Cheetah code is ideally suited to that purpose.

Acknowledgements

This work performed under the auspices of the U.S. Department of Energy by Lawrence Livermore National Laboratory under Contract DE-AC52-07NA27344.

References

1. Taylor, G. I., "The Dynamics of the Combustion Products Behind Plane and Spherical Detonation Fronts in Explosives", *Proceedings Royal Society, Series A*, **200**, pp. 235-247, 1950.
2. Zel'dovich, Ya. B., and Kompaneets, A. S., *Theory of Detonation*, Academic Press, New York, 284 pp., 1960 (originally published in Moscow in 1955).
3. Brode, H. L., "Blast Wave from a Spherical Charge", *Physics of Fluids*, **2** (2), pp. 217-229, 1959; also "Numerical Solutions of Spherical Blast Waves", *J. Appl. Phys.* **26**, p 766, 1955; also "A Calculation of the Blast Wave from a Spherical Charge of TNT", **RM-1965**, Rand Corp., Santa Monica, 1957.
4. Anisimov, S. I., and Zel'dovich, Ya. B., "Rayleigh-Taylor Instability of Boundary between Detonation Products and Gas in Spherical Explosion", *Pis'ma Zh. Eksp. Teor. Fiz.*, **3**, pp. 1081-1084, 1977.
5. Kuhl, A. L., "Spherical Mixing Layers in Explosions", *Dynamics of Exothermicity*, edited by J. R. Bowen, Gordon and Breach, Longhorn, PA, pp. 291-320 (+2 color plates), 1996.
6. Colella, P. & Glaz, H. M., "Efficient Solution Algorithms for the Riemann Problem for Real Gases", *J Comp. Phys.*, **59**, pp. 264-289, 1985.
7. Bell, J. B., Colella, P. & Trangenstein, J. A., "Higher Order Godunov Methods for General Systems of Hyperbolic Conservation Laws", *J Comp. Phys.*, **82** (2), pp. 362-397, 1989.
8. Bell, J., Berger, J. M., Saltzman, J., & Welcome, M. A., "Three-Dimensional Adaptive Mesh Refinement for Hyperbolic Conservation Laws", *SIAM J. Sci. Statist. Comput.*, **15** (1), pp. 127-138, 1994.
9. Colella, P., Ferguson, R. E., Glaz, H. M., & Kuhl, A. L. "Mach Reflection from an HE-driven Blast Wave". *Dynamics of Explosions: Progress in Astronautics and Aeronautics* **106** (ed. J. R. Bowen, J.-C. Leyer, R. I. Soloukhin), AIAA, pp. 388-421, 1986.

HOWARD & KUHL

10. Kinney, G. F., *Explosive Shocks in Air*, Macmillan Co, New York, 198 pp., 1962.
11. Baker, W. E., *Explosions in Air*, University of Texas Press, Austin, 268 pp., 1973.
12. Swisdak, M. M., *Explosion Effects and Properties—Part I: Explosion Effects In Air*, NSWC/WOL TR 75-116, 6 October 1975.
13. J. Petes, *Handbook of HE Explosion Effects*, DASIAC-TN-86-15, Defense Nuclear Agency, 1986, 42 pp.
14. Kuhl, A. L. & Reichenbach, H., Barometric Calorimeters, *ХИМИЧЕСКАЯ ФИЗИКА*, том 29, № 3, с. 1–8, 2010.
15. Kuhl, A. L. and Reichenbach, H. “Combustion Effects in Confined Explosions”, *Proceedings of the Combustion Institute* **32**, pp. 2291-2298, 2009.
16. A. L. Kuhl, J. B. Bell, V. E. Beckner, “Heterogeneous Continuum Model of Aluminum Particle Combustion in Explosions”, *Fizika Goreniya i Vzryva*, 2010 (in press).
17. Kuhl, A. L., Bell, J.B., Beckner, V. E., and Reichenbach, H. “Gasdynamic Model of Turbulent Combustion in TNT Explosions”, *33rd Combustion Symposium*, 2010 (accepted).
18. *Users Manual for ALE3D: an Arbitrary Lagrangian/Eulerian 2D and 3D code System*, A. L. Nicholls, Editor, **LLNL-SM-404490** (rev. 1), Lawrence Livermore National Laboratory, Livermore, CA., 2009.
19. L. E. Fried, *CHEETAH 1.22 User's Manual*, **UCRL-MA-117541** (rev. 2), LLNL, 187 pp., 1995.
20. Kuhl, A. L., “Thermodynamic states in Explosion Fields”, *14th Detonation Symposium*, April 2010 (accepted).
21. Mader, C. L., “Chapter 4C: Burning to Detonation”, *Numerical Modeling of Detonations*, pp. 266-268, University of California Press, Berkeley 1979.